Alexandria Engineering Journal (2020) 59, 565–577

HOSTED BY

Alexandria University

Alexandria Engineering Journal

www.elsevier.com/locate/aej
www.sciencedirect.com

ORIGINAL ARTICLE

Hall and ion slip effects on unsteady MHD free convective rotating flow through a saturated porous medium over an exponential accelerated plate

M. Veera Krishna [a,*], N. Ameer Ahamad [a,b], Ali J. Chamkha [c,d]

[a] Department of Mathematics, Rayalaseema University, Kurnool, Andhra Pradesh 518007, India
[b] Department of Mathematics, Faculty of Science, University of Tabuk, 71491, Saudi Arabia
[c] Department of Mechanical Engineering, Prince Sultan Endowment for Energy and Environment, Prince Mohammad Bin Fahd University, Al-Khobar 31952, Saudi Arabia
[d] RAK Research and Innovation Center, American University of Ras Al Khaimah, 10021, United Arab Emirates

Received 23 October 2019; revised 27 December 2019; accepted 21 January 2020

KEYWORDS

Inclined plate;
Rotation;
Hall and ion slip effects;
Radiation;
Chemical reaction;
Porous medium

Abstract In this paper, we have investigated the Hall and ion slip effects on the unsteady magnetohydrodynamic (MHD) free convective rotating flow over an exponentially accelerated inclined plate entrenched in a saturated porous medium with the effect of angle of inclination, variable temperature and concentration. The flow induced by the presence of heat source/sink and destructive reaction. The Laplace transform technique has been used to solve the governing equations. The effects of the non-dimensional parameters on the governing flow velocity, temperature and concentration are examined with graphical profiles. Also for engineering interest the shear stress, Nusselt number and Sherwood number are obtained analytically and discussed computationally with reference to foremost flow parameters. It is reported that the presence of magnetic field prevents the flow reversal. Angle of inclination sustains a retarding effect on velocity distribution. The present study has an immediate application in understanding the drag experienced at the heated and inclined surfaces in a seepage flow.
© 2020 Faculty of Engineering, Alexandria University. Production and hosting by Elsevier B.V. This is an open access article under the CC BY-NC-ND license (http://creativecommons.org/licenses/by-nc-nd/4.0/).

1. Introduction

Quick efforts have been made to learn the effects of porous media by both experimentally and theoretically. Simple flow is interested in the flow of water through agricultural engineering, groundwater sources and drainage, marine engineering, natural gas, oil, oil refining and refining processes. For petroleum extraction processes, it is important to stream porous media. In addition to contributing to existing knowledge,

* Corresponding author.
E-mail addresses: veerakrishna_maths@yahoo.com (M. Veera Krishna), n.ameer1234@gmail.com (N. Ameer Ahamad), achamkha@pmu.edu.sa (A.J. Chamkha).
Peer review under responsibility of Faculty of Engineering, Alexandria University.

https://doi.org/10.1016/j.aej.2020.01.043
1110-0168 © 2020 Faculty of Engineering, Alexandria University. Production and hosting by Elsevier B.V.
This is an open access article under the CC BY-NC-ND license (http://creativecommons.org/licenses/by-nc-nd/4.0/).

Nomenclature

u, v	the velocity components along x, y directions
$a*$	absorption coefficient
a	dimensionless accelerating parameter
a'	dimensional acceleration parameter
D	chemical molecular diffusivity
C	dimensional concentration in the fluid
C_w	concentration of the fluid near the plate
C_∞	concentration of the fluid far away from the plate
q_r	radiative heat flux
T	dimensional temperature of the fluid
T_w	constant temperature of the plate
T_∞	temperature of the fluid far away from the plate
S^*	constant heat source
K	permeability parameter
k	permeability of porous medium
Kc	chemical reaction parameter
Kc^*	chemical reaction rate constant
u_0	characteristic velocity of the plate
q	dimensionless complex velocity
Nu	Nusselt number
Sh	Sherwood number
Sc	Schmidt number
S	heat source parameter
M	magnetic field parameter or Hartmann number
C_p	specific heat at constant pressure
Gr	thermal Grashof number
Gm	mass Grashof number
g	acceleration due to gravity
Pr	Prandtl number
Ra	radiation parameter
B_0	applied magnetic field
k_1	thermal conductivity of the fluid
t	time
B	magnetic field vector
E	electric field
V	velocity vector
J	current density vector

Greek symbols

θ	dimensionless temperature
ϕ	dimension less fluid concentration
ν	coefficient of kinematic viscosity
ρ	density of the fluid
μ	coefficient of viscosity
β	volumetric coefficient of thermal expansion
$\beta*$	volumetric coefficient of expansion with concentration
σ	electrical conductivity
τ	shear stress
α	Angle of inclination from the vertical direction
ω_e	Cyclotron frequency
τ_e	Electron collision time
β_e	Hall parameter
β_i	ion slip parameter

many problems have significant practical significance. Porous materials used due to the efficiency of applied automated engineering, remediation and modern applications, as the principle of rolled liquid is very important because it used there are many natural events and a state worthy of being governed by the Corolis forces directly. The broad areas of Oceanography, Meteorology, Limnology and Atmospheric science all contain some important and essential features of rotating fluids.

The liquefied flow problems in rotating medium have drawn attention of many researchers who investigated hydrodynamic flow of a viscous and incompressible fluid in rotating medium considering different aspects of the problem. There has been considerable interest in the problems of hydromagnetic flow in a rotating environment during past few decades due to their geophysical and astrophysical significance and their application in fluid engineering. Several important problems, namely, maintenance and secular variations of terrestrial magnetic field due to motion in Earth's liquid core, internal rotation rate of the sun, structure of rotating magnetic stars, planetary and solar dynamo problems, MHD Ekman pumping, turbo machines, rotating hydromagnetic generators, rotating drum type separator in closed cycle two phase MHD generator flow etc. are directly governed by the action of Coriolis and magnetic forces. An order of magnitude analysis shows that, in the hydromagnetic equations of motion in rotating environment, the effects of Coriolis force is more significant than that of inertial and viscous forces. In addition to it, Coriolis and magnetic forces are comparable in magnitude. Some eminent authors [1–5] discussed the flow of electrically conducting liquids in different configurations.

Major interest of convective heat transfer of fluids in sciences and engineering is incredibly important. This is because of its wide variety of applications in the reproduction of cooling devices for microelectronic and electronic gear, solar energy anthology, etc. Water, ethylene glycol and engine oil are heating or cooling agents and play a decisive job in thermal management of many industries. In many realistic applications requiring strong magnetic field there is a need to think both the Hall and ion slip currents because of the significant effect they have on the vector of the current density and transitively on the magnetic force idiom. Ram [6] investigated the effects of Hall and ion slip currents on MHD rotating free convective heat generating flow. Seddeek [7] has discussed the effects of Hall and ion-slip currents and Heat transfer on magneto-micropolar fluid over a non-isothermal stretching sheet with suction and blowing. Seddeek and Abdelmeguid [8] discussed the boundary layer analysis which is used to the effects of Hall and ion slip currents on steady magneto-micropolar fluid over a horizontal plate. Jha and Apere [9] investigated unsteady MHD Couette flow of a Newtonian fluid between two rotating parallel plates taking Hall and ion-slip currents. Uddin and Kumar [10] discussed Hall and ion slip effect on thickness of the boundary layer flow of a micro polar fluid over a wedge. Ellahi et al. [11] conducted a theoretical study of the problem of the peristaltic flow of Jeffrey fluid in a non-uniform rectangular duct under the effects of Hall and ion slip. Bhatti et al. [12] discussed the effect of Hall and ion slip on peristaltic

blood flow of Eyring Powell in a non-uniform porous two dimensional channel under long wavelength approximation of zero Reynolds number. Srinivasacharya and Shafeeurrahman [13] discussed the Hall and ion slip effects on mixed convective flow of nanofluid between two concentric cylinders. Jitendra and Srinivasa [14] investigated the Hall and ion slip effects on convective flow of a rotating liquid.

Recently, the effects of radiation and Hall current on an unsteady MHD free convective flow in a vertical channel filled with a porous medium have been studied by Veera Krishna et al. [16]. The heat generation/absorption and thermo-diffusion on an unsteady free convective MHD flow of radiating and chemically reactive second grade fluid near an infinite vertical plate through a porous medium and taking the Hall current into account have been studied by Veera Krishna and Chamkha [17]. Veera Krishna et al. [18] discussed heat and mass-transfer effects on an unsteady flow of a chemically reacting micropolar fluid over an infinite vertical porous plate in the presence of an inclined magnetic field, Hall current and thermal radiation taken into account. Veera Krishna and Chamkha [19] discussed the MHD squeezing flow of a water-based nanofluid through a saturated porous medium between two parallel disks, taking the Hall current into account. Veera Krishna et al. [20] discussed Hall effects on MHD peristaltic flow of Jeffrey fluid through porous medium in a vertical stratum. Sara and Bhatti [21] investigated Nano fluid MHD peristaltic flow, including chemical reactions, Hall and ion slip currents. Veera Krishna and Chamkha [25] investigated The diffusion-thermo, radiation-absorption and Hall and ion slip effects on MHD free convective rotating flow of nanofluids past a semi-infinite permeable moving plate with constant heat source. Veera Krishna et al. [26] discussed the Soret and Joule effects of MHD mixed convective flow of an incompressible and electrically conducting viscous fluid past an infinite vertical porous plate taking Hall effects into account.

The natural convection of a Nano-encapsulated phase change materials suspension in a cavity with a hot wall having a time periodic temperature is investigated by Ahmad et al. [27]. Ghalambaz et al. [28] discussed the flow and thermal behavior of nano-encapsulated phase change materials dispersed in a liquid over a vertical flat plate. Hossein et al. [29] discussed numerically investigating convective boundary layer flow over a plate embedded in a porous medium filled with nanofluid. Aminreza et al. [30] investigated to analyze the boundary layer flow and heat transfer of nanofluids over a stretching sheet near the extrusion slit in the presence of variable thermal conductivity. Ghalambaz et al. [31] discussed melting flow and heat transfer of electrically conductive phase change materials subjecting to a non-uniform magnetic field in a square enclosure. Ghalambaz et al. [32] investigated the flow and heat transfer of MgO-MWCNTs/EG hybrid nanofluid in a complex shape enclosure filled with a porous medium. Ghalambaz et al. [33] are theoretically studied the MHD phase change heat transfer of a phase change substance in the presence of a uniform magnetic field in a cavity. The heat and mass transfer behavior of nanofluids inside a hexagonal enclosure in the presence of a non-uniform magnetic field considering the effects of ferro-hydrodynamic and MHD have been discussed by Ghalambaz et al. [34]. Double-diffusive convective flow in a rectangular enclosure with the upper and lower surfaces being insulated and impermeable is studied numerically by Mohamed [35]. Mohamed et al. [36] discussed double-diffusive natural convective flow in an inclined rectangular enclosure with the shortest sides being insulated and impermeable. Natural convection in a square cavity filled with different nanofluids is studied numerically by Mohamed and El-Maghlany [37]. Double-diffusive convective flow in an inclined rectangular enclosure with the shortest sides being insulated and impermeable is investigated numerically by Mohamed et al. [38].

The effects of chemical reaction on the MHD micropolar fluid stagnation-point flow through a stretching sheet with slip and convective boundary conditions are considered by Khilap et al. [39]. The heat transfer in MHD slip flow of an incompressible, viscous, electrically conducting, forced convective, and steady alumina-water nanofluid in the presence of a magnetic field over a flat plate has been analyzed by Padam et al. [40]. Alok and Manoj [41] discussed the effects of viscous dissipation and suction/injection on MHD flow of a nanofluid past a wedge with convective surface in the appearance of slip flow and porous medium. Himanshu et al. [42] are to identify the consequences of heat generation/absorption and suction/injection on MHD flow of Ag-water nanofluid past a stretching flat plat in a porous medium with Ohmic-viscous dissipation. Alok and Manoj [43] are discussed to analyze the MHD flow of Cu–water nanofluid between two stretchable/shrinking channels due to the effects of heat generation/absorption, viscous dissipation, and Ohmic heating. The collective influence of thermal radiation and convection flow of Cu-water nanofluid due to a stretching cylinder in a porous medium along with viscous dissipation and slip boundary conditions is examined by Alok and Manoj [44]. Ashish et al. [45] discussed the effect of slip parameters, viscous-Ohmic dissipation, heat generation/absorption, and suction/injection on MHD flow of silver-water nanofluid past a permeable vertical cone. Investigation of heat transfer effect on Cu-water nanofluid flow past a stretching cylinder has been done by Alok and Manoj [46].

Motivated by the data described above and literature survey bear witness that the analysis of Hall and ion effects of on the unsteady MHD free convection rotating flow over an exponentially accelerated inclined plate has not been presented yet. In order to fill the gap of the existing literature, we have investigated the Hall and ion slip effects on the unsteady MHD free convective rotating flow over an exponentially accelerated inclined plate entrenched in a saturated porous medium with the effect of angle of inclination, variable temperature and concentration.

2. Formulation and solution of the problem:

We have considered the Hall and ion slip effects on an unsteady uniform MHD free convective rotating flow of a viscous, incompressible and radiating fluid over an infinite exponentially accelerated inclined plate with variable temperature embedded in a saturated porous medium under the uniform transverse magnetic field of strengthB_0 normal to the plate. The x-axis is taken along the plate and z-axis is normal to the plate. The plate is inclined to vertical direction by an angle α. The induced magnetic field is neglected as the magnetic Reynolds number of the flow is very small. In an initially undisturbed state both the fluid and the plate are in rigid rotation

with the uniform angular velocity Ω about the normal to the plate. It is also assumed that the plate and the surrounding fluid are at the same temperature T_∞ and concentrationC_∞. At time $t > 0$, the plate is exponentially accelerated with a velocity $u = u_0 e^{a't}$, $v = 0$ in its own plane. At the same time the temperature and concentration level are also raised or lowered linearly with time t. The physical model of the problem is represented in Fig. 1.

The boundary layer equations of governing flow, heat and mass transfer over exponentially accelerated inclined plate (Bansal [23], Schlichting and Gersten [24]) are given by

$$\frac{\partial u}{\partial x} + \frac{\partial v}{\partial y} = 0 \tag{1}$$

$$\frac{\partial u}{\partial t} - 2\Omega v = v\frac{\partial^2 u}{\partial z^2} + \frac{B_0 J_y}{\rho} - \frac{v}{k}u + g\beta(T - T_\infty)\cos\alpha + g\beta^*(C - C_\infty)\cos\alpha \tag{2}$$

$$\frac{\partial v}{\partial t} + 2\Omega u = v\frac{\partial^2 v}{\partial z^2} - \frac{B_0 J_x}{\rho} - \frac{v}{k}v \tag{3}$$

$$\rho C_p \frac{\partial T}{\partial t} = k_1 \frac{\partial^2 T}{\partial z^2} - S^*(T - T_\infty) - \frac{\partial q_r}{\partial z} \tag{4}$$

$$\frac{\partial C}{\partial t} = D\frac{\partial^2 C}{\partial z^2} - \mathrm{Kc}^*(C - C_\infty) \tag{5}$$

The initial and boundary conditions are

$$u = 0, v = 0, T = T_\infty, C = C_\infty, \forall\ z,\quad t \leqslant 0 \tag{6}$$

$$u = u_0 e^{a't}, v = 0, T = T_\infty + \frac{(T_w - T_\infty)u_0^2 t}{\upsilon}, C = C_\infty + \frac{(C_w - C_\infty)u_0^2 t}{\upsilon} \quad \text{at}\ \ z = 0 \tag{7}$$

$$u = v = 0, T \to T_\infty, C \to C_\infty \quad \text{as} \quad z \to \infty \tag{8}$$

The boundary conditions for the temperature at the plate impose a linearity relation between temperature and time with a residual temperature T_∞ and having a constant slopeu_0^2/v,

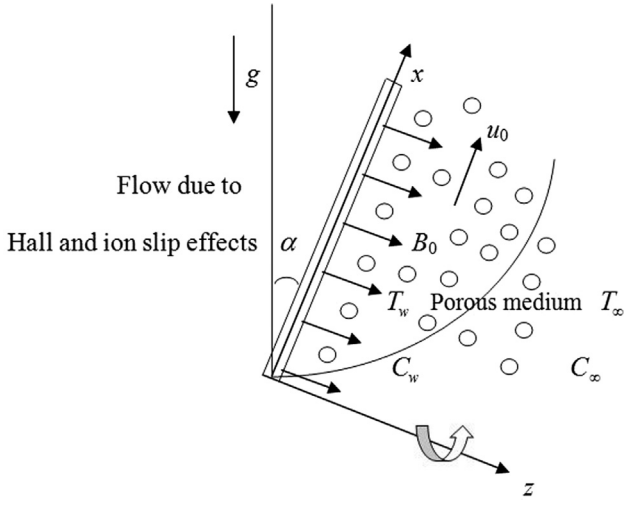

Fig. 1 Physical model.

which depends up on square of the characteristic velocity and material property. Similar explanation holds for concentration at the plate. The fluid considered here is a gray, absorbing/emitting radiation but a non-scattering medium. The local gradient for the case of an optically thin gray gas (Pattnaik et al. [22]) is expressed by

$$\frac{\partial q_r}{\partial z} = -4a^*\sigma(T_\infty^4 - T^4) \tag{9}$$

We assumed that the temperature differences within the flow are sufficiently small such that T^4 may be expressed as a linear function of the temperature. This is accomplished by expanding T^4 in a Taylor series about T_∞ and neglecting the higher order terms, we acquire that,

$$T^4 \cong 4T_\infty^3 T - 3T_\infty^4 \tag{10}$$

Using Eqs. (9) and (10) in (4), we get

$$\rho C_p \frac{\partial T}{\partial t} = k_1 \frac{\partial^2 T}{\partial z^2} - 16a^*\sigma T_\infty^3(T - T_\infty) + S^*(T - T_\infty) \tag{11}$$

The electron-atom collision frequency is assumed to be very high, so that Hall and ion slip currents cannot be neglected. Hence, the Hall and ion slip currents give rise to the velocity in y-direction. When the strength of the magnetic field is very large, the generalized Ohm's law is modified to include the Hall and ion slip effect (Sutton and Sherman [15]),

$$J = \sigma(E + V \times B) - \frac{\omega_e \tau_e}{B_0}(J \times B) + \frac{\omega_e \tau_e \beta_i}{B_0^2}((J \times B) \times B)) \tag{12}$$

Further it is assumed that $\omega_e\tau_e \sim O(1)$ and $\omega_i\tau_i << 1$, in the Eq. (9), the electron pressure gradient and thermo-electric effects are neglected, *i.e.*, the electric field $E = 0$ under these assumptions, the Eq. (12) reduces to

$$(1 + \beta_i\beta_e)J_x + \beta_e J_y = \sigma B_0 v \tag{13}$$

$$(1 + \beta_i\beta_e)J_y - \beta_e J_x = -\sigma B_0 u \tag{14}$$

On solving Eqs. (12) and (13) we obtain,

$$J_x = \sigma B_0(\alpha_{22}u + \alpha_{11}v) \tag{15}$$

$$J_y = -\sigma B_0(\alpha_{22}v - \alpha_{11}u) \tag{16}$$

where, $\alpha_{11} = \frac{1+\beta_e\beta_i}{(1+\beta_e\beta_i)^2+\beta_e^2}$ and $\alpha_{22} = \frac{\beta_e}{(1+\beta_e\beta_i)^2+\beta_e^2}$

Substituting the Eqs. (15) and (16) in (3) and (2) respectively, we obtain

$$\frac{\partial u}{\partial t} - 2\Omega v = v\frac{\partial^2 u}{\partial z^2} + \frac{\sigma B_0^2(\alpha_{22}v - \alpha_{11}u)}{\rho} - \frac{v}{k}u + g\beta(T - T_\infty)\cos\alpha + g\beta^*(C - C_\infty)\cos\alpha \tag{17}$$

$$\frac{\partial v}{\partial t} + 2\Omega u = v\frac{\partial^2 v}{\partial z^2} - \frac{\sigma B_0^2(\alpha_{22}u + \alpha_{11}v)}{\rho} - \frac{v}{k}v \tag{18}$$

Combining the Eqs. (17) and (18)

$$\frac{\partial q}{\partial t} + 2i\Omega q = v\frac{\partial^2 q}{\partial z^2} - \frac{\sigma B_0^2(\alpha_{11} + i\alpha_{22})}{\rho}q - \frac{v}{k}q + g\beta(T - T_\infty)\cos\alpha + g\beta^*(C - C_\infty)\cos\alpha \tag{19}$$

On introducing the following non-dimensional quantities

$$z^* = \frac{zu_0}{v}, q^* = \frac{q}{u_0}, t^* = \frac{tu_0^2}{v}, a = \frac{a'v}{u_0^2}, \theta = \frac{T - T_\infty}{T_w - T_\infty},$$

$$\phi = \frac{C - C_\infty}{C_w - C_\infty}, \mathrm{Gr} = \frac{g\beta v(T_w - T_\infty)}{u_0^3}, \mathrm{Pr} = \frac{\mu C_p}{k_1},$$

$$\mathrm{Gm} = \frac{g\beta^* v(C_w - C_\infty)}{u_0^3}, M = \frac{\sigma B_0^2 v}{\rho u_0^2}, K = \frac{u_0^2 k}{v^2}, \mathrm{Kc} = \frac{v\mathrm{Kc}*}{u_0^2},$$

$$\mathrm{Ra} = \frac{16a^* v^2 \sigma T_\infty}{k_1 u_0^2}, S = \frac{S^* v}{\rho C_p u_0^2},$$

$$\mathrm{Sc} = \frac{v}{D}, R = \frac{2\Omega v}{u_0^2}$$

Making use of non-dimensional variables, the governing equations reduces to (Dropping asterisks)

$$\frac{\partial q}{\partial t} = \frac{\partial^2 q}{\partial z^2} - \left(M^2(\alpha_{11} + i\alpha_{22}) + 2iR + \frac{1}{K}\right)q + \mathrm{Gr}\theta\cos\alpha + \mathrm{Gm}\phi\cos\alpha \tag{20}$$

$$\frac{\partial \theta}{\partial t} = \frac{1}{\mathrm{Pr}}\frac{\partial^2 \theta}{\partial z^2} - \left(\frac{Ra}{\mathrm{Pr}} - S\right)\theta \tag{21}$$

$$\frac{\partial \phi}{\partial t} = \frac{1}{\mathrm{Sc}}\frac{\partial^2 \phi}{\partial z^2} - \mathrm{Kc}\phi \tag{22}$$

The initial and boundary conditions in dimensionless are

$$q = 0, \theta = 0, \phi = 0, \forall z, t \leqslant 0 \tag{23}$$

$$q = e^{at}, \theta = t, \phi = t \quad \text{at} \quad z = 0 \tag{24}$$

$$q \to 0, \theta \to 0, \phi \to 0 \quad \text{as} \quad z \to \infty \tag{25}$$

Taking Laplace transform of equations (20), (21) and (22), we get

$$\frac{d^2\overline{q}}{dz^2} - \left(s + M^2(\alpha_{11} + i\alpha_{22}) + 2iR + \frac{1}{K}\right)\overline{q} = \frac{\mathrm{Grcos}\alpha}{s^2}e^{-\mathrm{Pr}(s+(R/\mathrm{Pr})-S)z} + \frac{\mathrm{Gmcos}\alpha}{s^2}e^{-\mathrm{Sc}(s+\mathrm{Kc})z} \tag{26}$$

$$\frac{d^2\overline{\theta}}{dz^2} - \mathrm{Pr}\left(s + \frac{Ra}{\mathrm{Pr}} - S\right)\overline{\theta} = 0 \tag{27}$$

$$\frac{d^2\overline{\phi}}{dz^2} - \mathrm{Sc}(s + \mathrm{Kc})\overline{\phi} = 0 \tag{28}$$

Corresponding transformed boundary conditions are,

$$\overline{q} = \frac{1}{s-a}, \overline{\theta} = \frac{1}{s^2}, \overline{\phi} = \frac{1}{s^2} \text{ at } z = 0 \tag{29}$$

$$\overline{q} \to 0, \overline{\theta} \to 0, \overline{\phi} \to 0 \text{ as } z \to \infty \tag{30}$$

Solving the Eqs. (26), (27), and (28) by making use of (29) and (30), we obtained transformed solutions for $\overline{q}$, $\overline{\theta}$ and $\overline{\phi}$ are,

$$\begin{aligned}\overline{q}(z,s) = {} & \left\{\frac{1}{s-a} - \frac{1}{\left(\mathrm{Pr}\left(s + \frac{\mathrm{Ra}}{\mathrm{Pr}} - S\right)\right)^2 - \lambda_3^2}\frac{\mathrm{Grcos}\alpha}{s^2} - \frac{1}{(\mathrm{Sc}(s+\mathrm{Kc}))^2 - \lambda_3^2}\frac{\mathrm{Gmcos}\alpha}{s^2}\right\} \\ & + \frac{1}{\left(\mathrm{Pr}\left(s + \frac{\mathrm{Ra}}{\mathrm{Pr}} - S\right)\right)^2 - \lambda_3^2}\frac{\mathrm{Grcos}\alpha}{s^2}e^{-(\mathrm{Pr}(s+(R/\mathrm{Pr})-S))z}e^{-\lambda_3 z} \\ & + \frac{1}{\left(\mathrm{Pr}\left(s + \frac{\mathrm{Ra}}{\mathrm{Pr}} - S\right)\right)^2 - \lambda_3^2}\frac{\mathrm{Grcos}\alpha}{s^2}e^{-(\mathrm{Pr}(s+(R/\mathrm{Pr})-S))z} \\ & + \frac{1}{(\mathrm{Sc}(s+\mathrm{Kc}))^2 - \lambda_3^2}\frac{\mathrm{Gmcos}\alpha}{s^2}e^{-(\mathrm{Sc}(s+\mathrm{Kc}))z}\end{aligned} \tag{31}$$

$$\overline{\theta}(z,s) = \frac{1}{s^2}e^{-\mathrm{Pr}(s+(\mathrm{Ra}/\mathrm{Pr})-S)z} \tag{32}$$

$$\overline{\phi}(z,s) = \frac{1}{s^2}e^{-\mathrm{Sc}(s+\mathrm{Kc})z} \tag{33}$$

Taking inverse Laplace transforms to the equations (31), (32), and (33), we obtained velocity, temperature and concentration distributions. The shear stress, Nusselt number and Sherwood number are obtained as,

$$\tau = -\left(\frac{\partial q}{\partial z}\right)_{z=0}$$

$$Nu = -\left(\frac{\partial \theta}{\partial z}\right)_{z=0} \quad \text{and} \quad \mathrm{Sh} = -\left(\frac{\partial \phi}{\partial z}\right)_{z=0} \tag{34}$$

The expressions are cited in the Appendix A.

3. Results and discussion

The investigation of the graphical depiction of flow, heat and mass transfer phenomena brings out the effects of different parameters on governing the flow. The Figs. 2–5, 6 and 7 characterize the resultant velocity, temperature and concentration distributions respectively. The validation of the results is shown in Table 1. Table 2, Figs. 8 and 9 illustrated the shear stress, Nusselt number and Sherwood number respectively. For $a = 0$in Eq. (24), the plate is set to a constant motion. It is also evident from boundary condition that elapse of time induces higher start-up for $a > 0$in velocity, temperature and concentration distributions. For computational purpose, we are fixing $t = 0.5$ while the parameters $M = 0.5$, $K = 1$, $\mathrm{Kc} = 1$, $\mathrm{Gr} = 3$, $\mathrm{Gm} = 2$, $\mathrm{Sc} = 0.22$, $\mathrm{Pr} = 0.71$, $S = 1$, $Ra = 2$, $\alpha = \pi/6$, $a = 0.2$, $t = 0.5$, $\beta_e = 0.2$, $\beta_i = 1$, and $R = 0.5$ are varied over the range.

Fig. 2(a and d) exhibits the resultant velocity profiles with Hartmann number M, permeability parameter K, thermal Grashof number Gr and mass Grashof number Gm. It is seen from Fig. 2(a) that sudden decrement in velocity is observed near the plate in the presence of magnetic field. It is also seen that their presence reduces the velocity field at all points. This is due to the fact that the introduction of a transverse magnetic field, normal to the flow direction, has a tendency or affinity to create the drag known as the Lorentz force which tends to resist the flow throughout the fluid region. Thus, it is concluded that the effect of magnetic field in the presence of porous matrix, sustains a retarding effect on the velocity distribution and thickness of the momentum boundary layer.

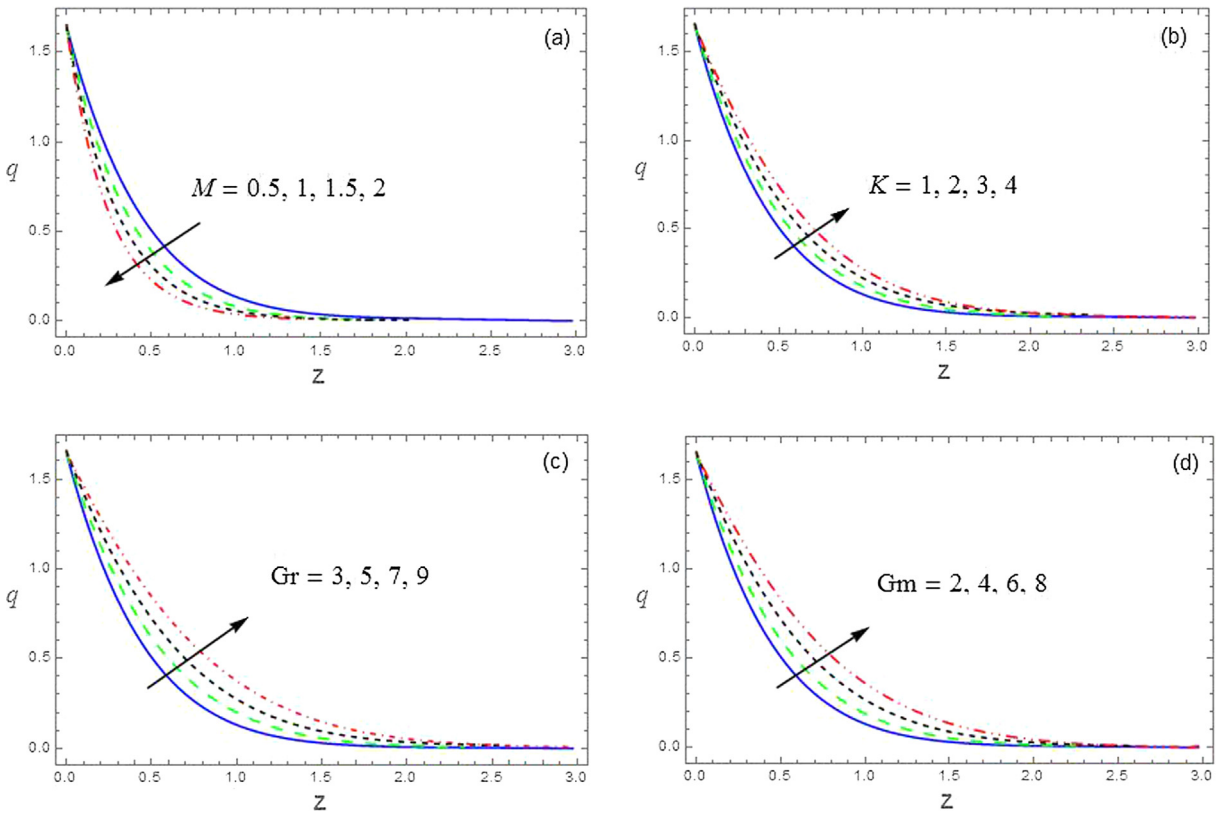

Fig. 2 The velocity profiles against *M*. *K*, Gr and Gm.

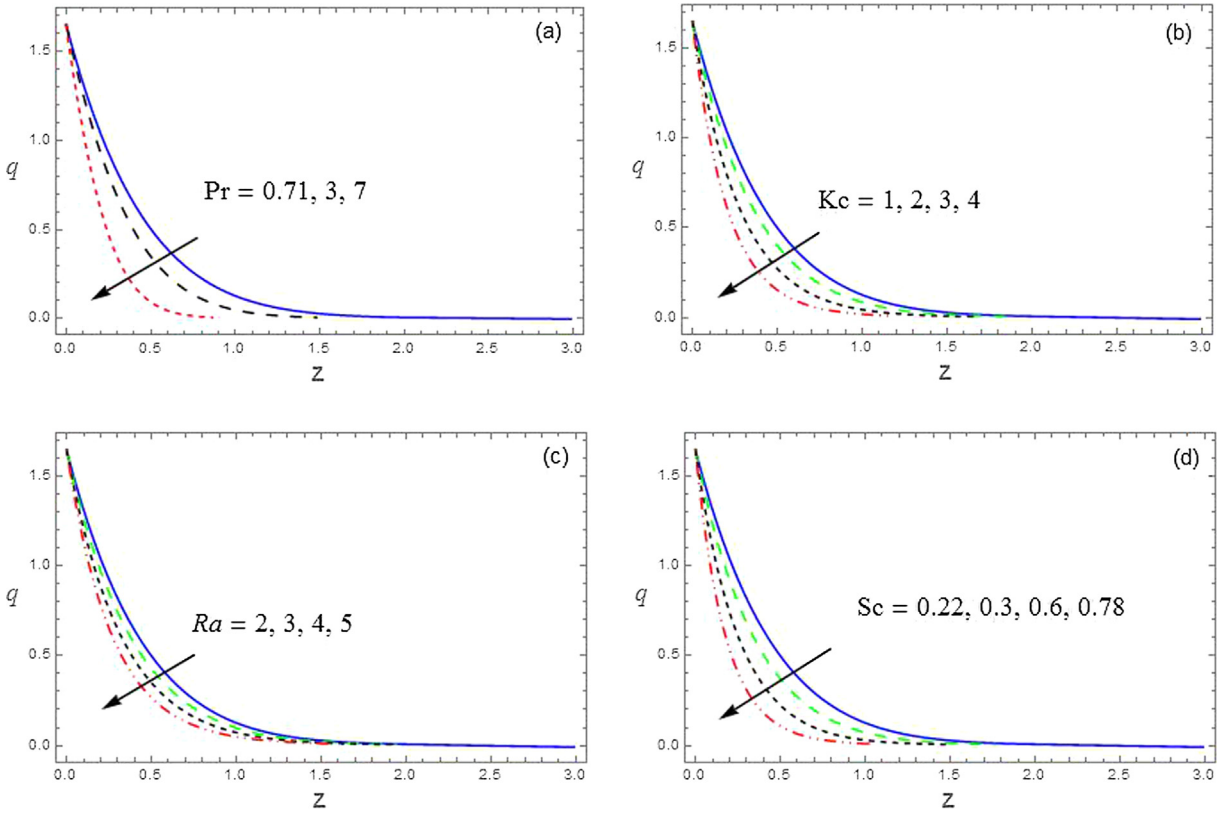

Fig. 3 The velocity profiles against Pr, Kc, *Ra* and Sc.

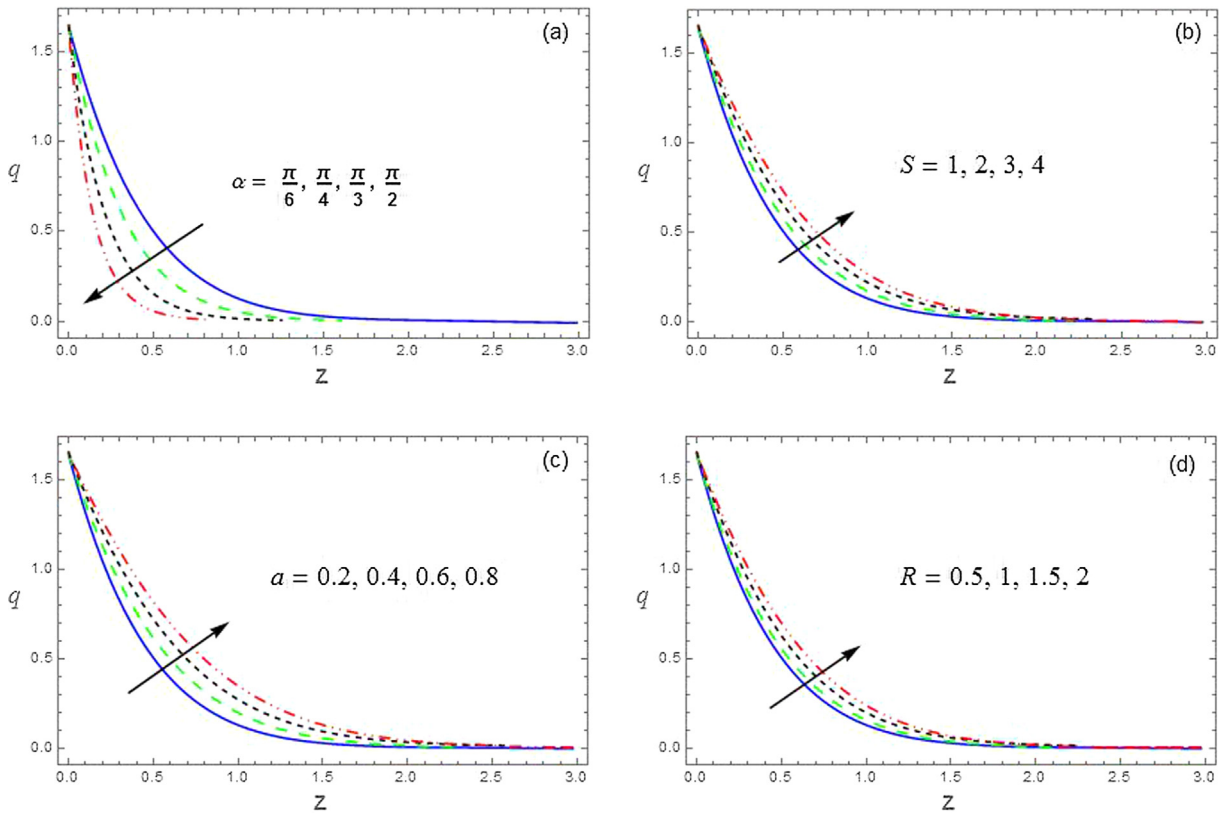

Fig. 4 The velocity profiles against α, S, a and R.

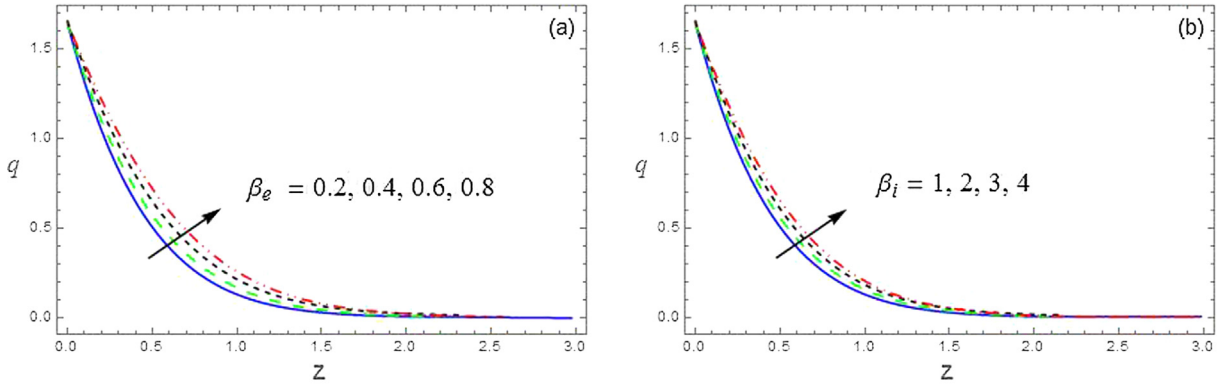

Fig. 5 The velocity profiles against β_e and β_i.

For different values of the permeability parameter K, the velocity distribution is plotted in Fig. 2(b). It is clear that the increased values K increase the resultant velocity and thereby increase the momentum boundary layer thickness. Lower the permeability causes lesser the fluid speed is observed within the flow region occupied by the fluid. Hence the resultant velocity enhances with increasing permeability parameter throughout the fluid section. The resultant velocity across the boundary layer increases with increasing thermal Grashof number Gr (Fig. 2(c)). The thermal Grashof number Gr signifies the relative effect of the thermal buoyancy force to the viscous hydrodynamic force in the boundary layer. As expected, it is observed that there is a rise in the velocity due to the enhancement of thermal buoyancy force. It is concluded that increase in the value of Grashof number or any buoyancy related parameter implies an increase in the wall temperature and this makes the bond between the fluid to become weaker, strength of the internal friction to decrease, the gravity to becomes stronger enough. *i.e.*, makes the specific weight appreciably different between the immediate fluid layers adjacent to the wall. The effects of buoyancy parameter are highly significant in the flow within the boundary layer formed on the surface. This is only achievable when the prescribed surface temperature and prescribed wall heat flux are considered. Similar behaviour is observed with increasing mass Grashof number Gm (Fig. 2(d). The mass Grashof number Gc defines the

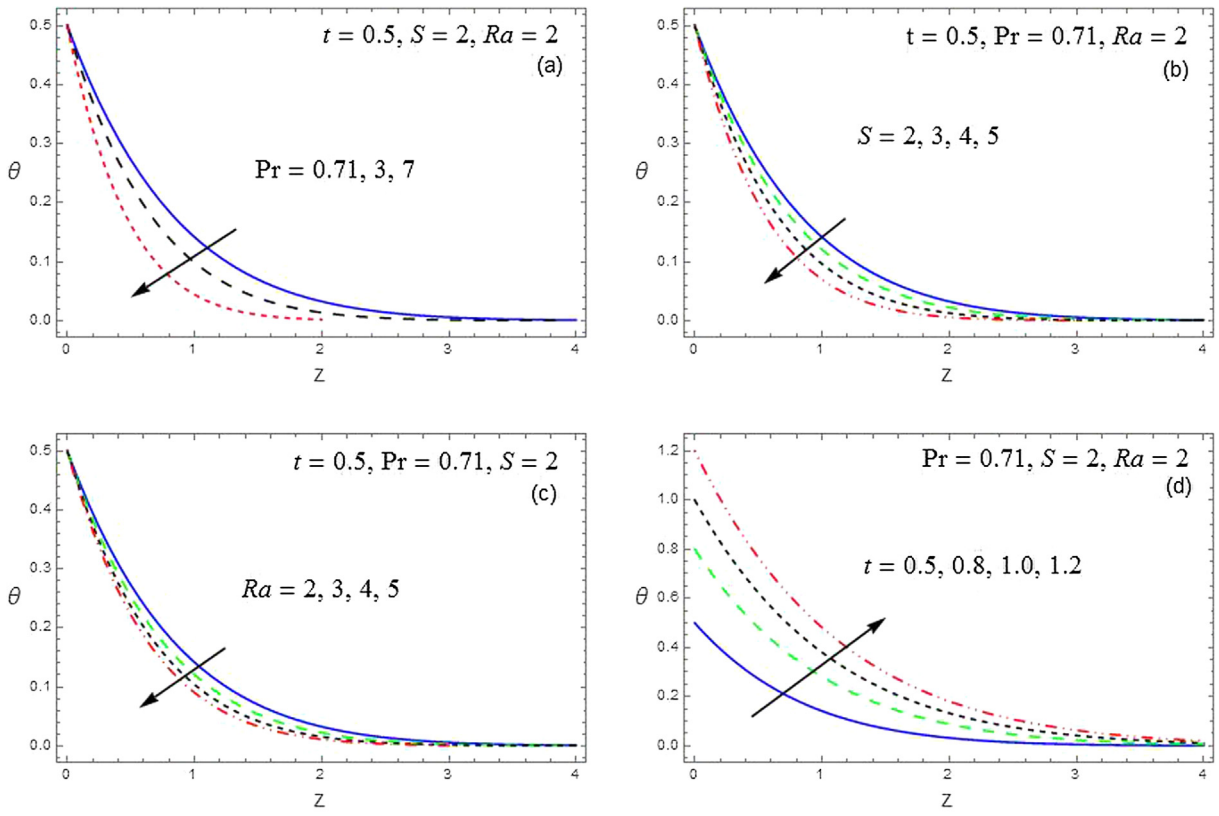

Fig. 6 The temperature profiles against Pr, S, Ra and t.

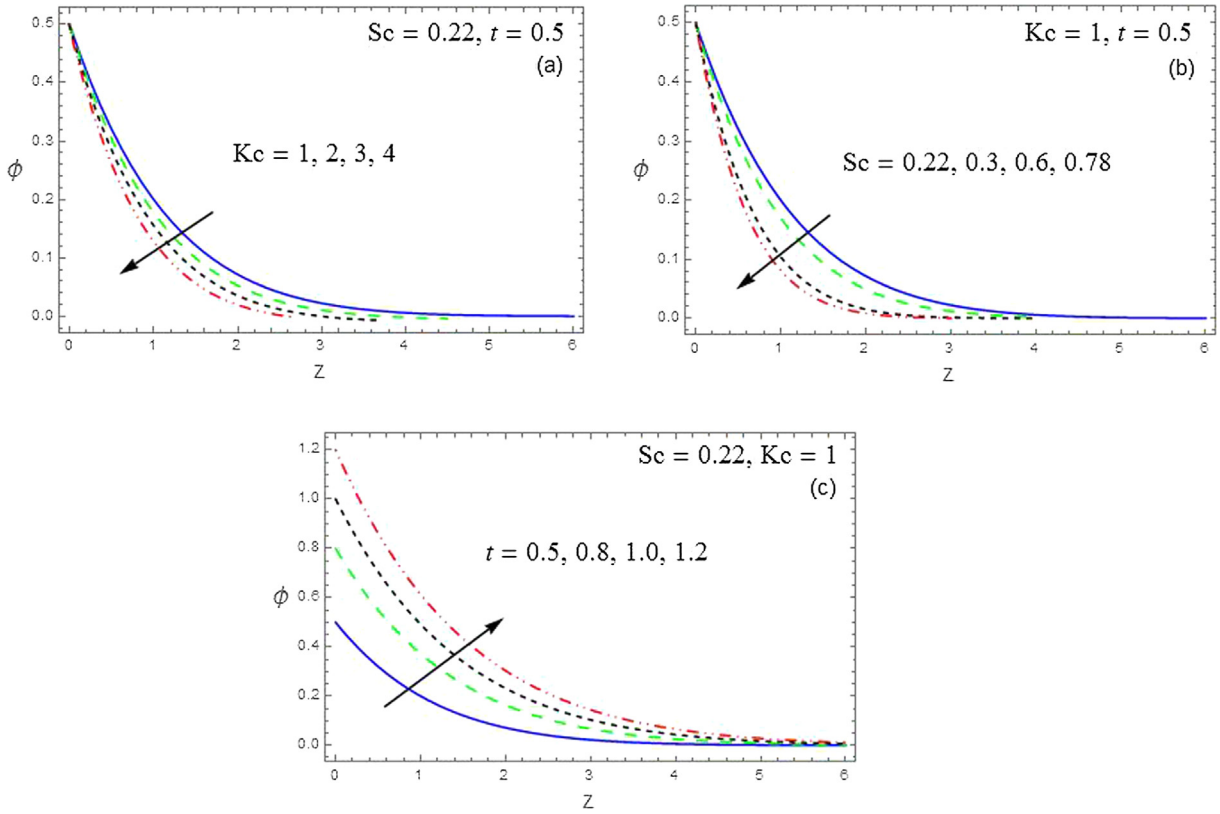

Fig. 7 The concentration profiles against Kc, Sc and t.

Table 1 Results comparison for the velocity component (u) (Kc = 1, Sc = 0.22, Pr = 0.71, Gr = 3, Gm = 2, $\alpha = \pi/6$, $a = 0.2, t = 0.5, z = 0.5, R = 0, \beta_e = \beta_i = 0$).

M	K	S	Ra	Previous work Pattnaik et al. [22]	Present Work
0.5	1	1	2	0.671987	0.671989
1.0				0.610769	0.610770
1.5				0.527190	0.527191
	2			0.668627	0.668626
	3			0.579948	0.579947
		2		0.676540	0.676539
		3		0.681819	0.681820
			3	0.666571	0.666570
			4	0.662057	0.662058

Table 2 Shear stress.

M	K	Gr	Gm	Pr	Kc	Ra	Sc	α	S	a	R	β_e	β_i	τ
0.5	**1**	**3**	**2**	**0.71**	**1**	**2**	**0.22**	$\pi/6$	**1**	**0.2**	**0.5**	**0.2**	**1**	1.51115
1														1.68936
1.5														1.96947
	2													1.42771
	3													1.34569
		5												1.45149
		7												1.39183
			4											1.43536
			6											1.35956
				3										1.53727
				6										1.55234
					2									1.51206
					3									1.51292
						3								1.51321
						4								1.51513
							0.3							1.51498
							0.6							1.52414
								$\pi/4$						1.54149
								$\pi/3$						1.58102
									2					1.50960
									3					1.50796
										0.4				1.62908
										0.6				1.75321
											1			1.24167
											1.5			1.03331
												0.4		1.48557
												0.6		1.44589
													2	1.42254
													3	1.33325

Note: Bold face values represent the variation of particular parameter being other parameters fixed.

ratio of the species buoyancy force to the viscous hydrodynamic force. The fluid resultant velocity increases and is more distinctive due to increase in the species buoyancy force. The velocity distribution attains a distinctive maximum value within the fluid medium and then decreases properly to approach zero. Thus momentum boundary layer thickness increases with increase in Gr or Gm.

We noticed from the Fig. 3(a and d), this exhibits the effect of Prandtl number Pr, chemical reaction parameter Kc, radiation parameter *Ra* and Schmidt number Sc on resultant velocity. The increase in Prandtl number decreases the velocity throughout the fluid region. Hence momentum boundary layer reduces with increasing Prandtl number (Fig. 3(a)). Similar behaviour is observed with increasing chemical reaction parameter Kc or radiation parameter *Ra* (Fig. 3(b and c)). Heavier diffusing species, i.e. with higher value of Schmidt number and increasing rate of chemical reaction cause a reduction in velocity. Moreover, heavier species with destructive reaction causes retardation in the velocity distribution (Fig. 3 (d)).

Fig. 4(a and d) shows the effect of angle of inclination of the plate. It is further remarked that an increase in angle of

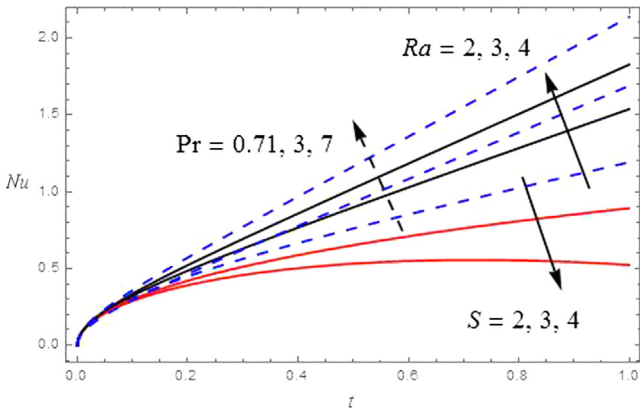

Fig 8 Nusselt number with Pr, *Ra* and *S*.

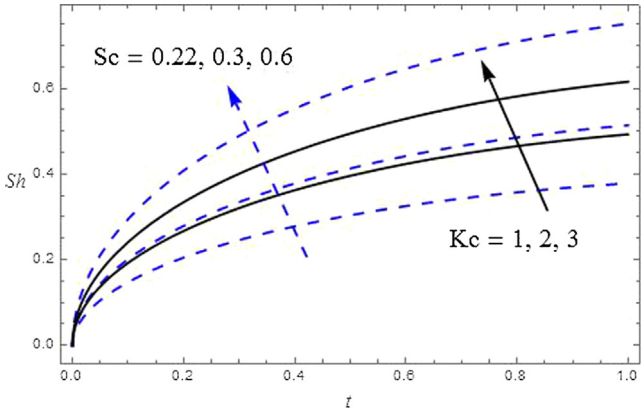

Fig 9 Sherwood number with Kc and Sc.

inclination reduces the velocity at all points, as the forcing forces are depleted due to the factor cosα (Fig. 4(a)). It is observed that in the presence of constant rotation, an increase in heat source parameter leads to an increase in the velocity at all points, but reverse effect is observed in respect of acceleration parameter (Fig. 4(b and c)). Thus, the presence of heat source is found to be favourable in enhancing the velocity. The resultant velocity enhances with increasing rotation parameter R (Fig. 4(d)). This may be attributed to the fact that when the frictional layer at the plate is suddenly set into the motion then the Coriolis force acts as a freedom in the entire fluid flow region.

Fig. 5(a and b) exhibits the effect of Hall and ion slip parameters β_e and β_i. The resultant velocity increases with increasing Hall parameter (Fig. 5(a)). The inclusion of Hall parameter β_e reduces the effective conductivity and hence drops the magnetic resistive force. The similar behaviour is observed with increasing ion slip parameter β_i(Fig. 5(b)). The effective conductivity increases as increase in β_i, hence the damping force is decreasing due to this axial velocity increases.

The smooth distinction of temperature is marked throughout the flow domain in the Fig. 6(a and d). We increase in Prandtl number Pr, i.e., fluid with low thermal diffusivity and with an increasing strength of heat source, decreases the temperature slightly at all points. It is to note that the velocity decreases in the presence of heat source parameter (Fig. 6(a and b)). An increase in radiation parameter decreases the temperature. From the boundary condition it is evident that the plate temperature equals to the time. Therefore, an elapse of time leads to higher temperature on the plate (Fig. 6(c and d)).

Further, variation of concentration in the flow domain is depicted through Fig. 7(a–c). From Fig. 7(a), an increase in the chemical reaction parameter Kc decreases the concentration profile rapidly. Since, the number of solute molecules undergoing chemical reaction gets increased as chemical reaction parameter increases, which lead to decrease in concentration field. Hence, a destructive chemical reaction reduces the concentration boundary layer thickness significantly. It is observed from Fig. 7(b) that high value of Schmidt number i.e., heavier species with low diffusivity decrease the concentration at all points of the flow domain. An increase in the Schmidt number corresponds to a weaker solute diffusivity which allows a shallower dispersion of solutal effect. As a result, the concentration decreases with increase in Schmidt number. Thus, the conentration boundary layer is thicker for smaller values of Schmidt number and vice versa. We chose the Schmidt number values as Sc = 0.22, 0.3, 0.6, 0.78 which correspond to hydrogen, helium, water vapour, and ammonia respectively. Further, it is observed that the concentration of profile becomes steeper in the presence of chemical reaction. Reversal behaviour is observed with increasing time throughout the fluid region (Fig. 7(c)).

The Shear stress, Nusselt number and Sherwood number feature breaking point surface area which is important for flow dependence, warmth and adhesive. As can be found in Table 2, it is observed that the shear stress decreases with an increase in the values of permeability parameter, heat source parameter, rotation parameter, Hall and ion slip effects as well as thermal and mass buoyancy parameter and it increases with increasing Hartmann number, Prandtl number, chemical reaction parameter, radiation parameter, Schmidt number, angle of inclination and accelerated parameter. In Fig. 8, we noticed that Nusselt number increases with increasing Prandtl number, radiation parameter and time, whereas, it decreases with heat source parameter. Thus, it is concluded that the fluid with higher radiative property and low thermal diffusivity favours higher rate of heat transfer at the surface. From Fig. 9, it is observed that Sherwood number, which determines the rate of solutal concentration at the surface of the wall, increases with increasing Schmidt number, chemical reaction parameter and time. Thus, heavier species with higher rate of chemical reaction increases the rate of solutal concentration at the surface.

4. Conclusions

We have investigated the Hall and ion slip effects on the unsteady MHD free convective flow over an exponentially accelerated inclined plate entrenched in a saturated porous medium with the effect of angle of inclination, variable temperature and concentration. The conclusions are made as follows. Presence of Hall and ion slip effects and saturated porous medium offers capitulate to the increase of velocity distribution thereby acts as a over protective device for preventing front flow. The angle of inclination, the chemical reaction and the presence of heavy species have resistance to velocity.

The combined effects of rotation, Hall and ion slip accelerates the fluid motion. An increase in radiation parameter decreases the temperature so as to reach the ambient state earlier. The low diffusing species with higher rate of chemical reaction diminishes the concentration level at all points. Increasing the rate of chemical reaction increases the shear stress and reduces it by increasing permeability parameter, which is advantageous. The presence of porous matrix and free convective flow reduces the shear stress, while other parameters increase it. Flow instability is noticeable due to long duration. Nusselt number enhances with increasing radiation and retards with increasing heat source. Sherwood number increases with increasing Schmidt number, chemical reaction parameter and time.

Declaration of Competing Interest

The authors declare that they have no known competing financial interests or personal relationships that could have appeared to influence the work reported in this paper.

Appendix A.

$$\lambda = M^2(\alpha_{11} + i\alpha_{22}) + 2iR + \frac{1}{K},\ d = Ra - S\mathrm{Pr},\ \alpha_1 = \frac{(\mathrm{Ra} - \lambda - S\mathrm{Pr})}{1 - \mathrm{Pr}},\ \alpha_2 = \frac{(\mathrm{ScKc} - \lambda)}{1 - \mathrm{Sc}},$$

$$\lambda_1^2 = \mathrm{Sc}(s + \mathrm{Kc}),\ \lambda_2^2 = \mathrm{Pr}\left(s + \frac{\mathrm{Ra}}{\mathrm{Pr}} - S\right),\ \lambda_3^2 = s + M^2(\alpha_{11} + i\alpha_{22}) + 2\mathrm{iR} + \frac{1}{K}.$$

$$q(z,t) = \left(\frac{e^{at}}{2}\right)\left(e^{(z\sqrt{\lambda+a})}erfc\left(\frac{z}{2\sqrt{t}} + \sqrt{(\lambda+a)t}\right) + e^{(-z\sqrt{\lambda+a})}erfc\left(\frac{z}{2\sqrt{t}} - \sqrt{(\lambda+a)t}\right)\right)$$

$$+\left(\frac{\mathrm{Grcos}\alpha}{2(\mathrm{Pr}-1)}\right)\left(\frac{e^{(\alpha_1 t)}}{\alpha_1^2}\left\{e^{(z\sqrt{\lambda+\alpha_1})}erfc\left(\frac{z}{2\sqrt{t}} + \sqrt{(\lambda+\alpha_1)t}\right) + e^{(-z\sqrt{\lambda+\alpha_1})}erfc\left(\frac{z}{2\sqrt{t}} - \sqrt{(\lambda+\alpha_1)t}\right)\right.\right.$$

$$\left.\left. -e^{(-z\sqrt{(d+\mathrm{Pr}\alpha_1)})}erfc\left(\frac{z}{2}\sqrt{\frac{\mathrm{Pr}}{t}} - \sqrt{\left(\frac{d}{\mathrm{Pr}} + \alpha_1\right)t}\right)\right\} - e^{(-z\sqrt{(d+\mathrm{Pr}\alpha_1)})}erfc\left(\frac{z}{2}\sqrt{\frac{\mathrm{Pr}}{t}} - \sqrt{\left(\frac{d}{\mathrm{Pr}} + \alpha_1\right)t}\right)\right\}$$

$$-\frac{1}{\alpha_1}\left(t + \frac{1}{\alpha_1} + \frac{z}{2\sqrt{\lambda}}\right)e^{(z\sqrt{\lambda})}erfc\left(\frac{z}{2\sqrt{t}} + \sqrt{\lambda t}\right) - \frac{1}{\alpha_1}\left(t + \frac{1}{\alpha_1} - \frac{z}{2\sqrt{t}}\right)e^{(-z\sqrt{\lambda})}erfc\left(\frac{z}{2\sqrt{t}} - \sqrt{\lambda t}\right)$$

$$+\frac{1}{\alpha_1}\left(t + \frac{1}{\alpha_1} + \frac{z\mathrm{Pr}}{2\sqrt{d}}\right)e^{(z\sqrt{d})}erfc\left(\frac{z}{2}\sqrt{\frac{\mathrm{Pr}}{t}} + \sqrt{\frac{dt}{\mathrm{Pr}}}\right) + \frac{1}{\alpha_1}\left(t + \frac{1}{\alpha_1} - \frac{z\mathrm{Pr}}{2\sqrt{d}}\right)e^{(-z\sqrt{d})}erfc\left(\frac{z}{2}\sqrt{\frac{\mathrm{Pr}}{t}} - \sqrt{\frac{dt}{\mathrm{Pr}}}\right)\right)$$

$$+\left(\frac{\mathrm{Gmcos}\alpha}{2(\mathrm{Sc}-1)}\right)\left(\frac{e^{(\alpha_2 t)}}{\alpha_2^2}\left\{e^{(z\sqrt{\lambda+\alpha_2})}erfc\left(\frac{z}{2\sqrt{t}} + \sqrt{(\lambda+\alpha_2)t}\right) + e^{(-z\sqrt{(\lambda+\alpha_2)t})}erfc\left(\frac{z}{2\sqrt{t}} - \sqrt{(\lambda+\alpha_2)t}\right)\right.\right.$$

$$\left.\left. -e^{(z\sqrt{\mathrm{Sc}(\mathrm{Kc}+\alpha_2)})}erfc\left(\frac{z}{2}\sqrt{\frac{\mathrm{Sc}}{t}} + \sqrt{(\mathrm{Kc}+\alpha_2)t}\right) - e^{(-z\sqrt{\mathrm{Sc}(\mathrm{Kc}+\alpha_2)})}erfc\left(\frac{z}{2}\sqrt{\frac{\mathrm{Sc}}{t}} - \sqrt{(\mathrm{Kc}+\alpha_2)t}\right)\right\}\right.$$

$$-\frac{1}{\alpha_2}\left(t + \frac{1}{\alpha_2} + \frac{z}{2\sqrt{\lambda}}\right)e^{(z\sqrt{\lambda})}erfc\left(\frac{z}{2\sqrt{t}} + \sqrt{\lambda t}\right) - \frac{1}{\alpha_2}\left(t + \frac{1}{\alpha_2} - \frac{z}{2\sqrt{\lambda}}\right)e^{(-z\sqrt{\lambda})}erfc\left(\frac{z}{2\sqrt{t}} - \sqrt{\lambda t}\right)$$

$$+\frac{1}{\alpha_2}\left(t + \frac{1}{\alpha_2} + \frac{z}{2}\sqrt{\frac{\mathrm{Sc}}{\mathrm{Kc}}}\right)e^{(z\sqrt{\mathrm{ScKc}})}erfc\left(\frac{z}{2}\sqrt{\frac{\mathrm{Sc}}{t}} + \sqrt{\mathrm{Kc}t}\right) + \frac{1}{\alpha_2}\left(t + \frac{1}{\alpha_2} - \frac{z}{2}\sqrt{\frac{\mathrm{Sc}}{\mathrm{Kc}}}\right)e^{(-z\sqrt{\mathrm{ScKc}})}erfc\left(\frac{z}{2}\sqrt{\frac{\mathrm{Sc}}{t}} - \sqrt{\mathrm{Kc}t}\right)\right)$$

$$\theta(z,t) = \frac{1}{2}\left(\left(t + \frac{z\mathrm{Pr}}{2\sqrt{d}}\right)e^{(z\sqrt{d})}erfc\left(\frac{z}{2}\sqrt{\frac{\mathrm{Pr}}{t}} + \sqrt{\frac{dt}{\mathrm{Pr}}}\right) + \left(t - \frac{z\mathrm{Pr}}{2\sqrt{d}}\right)e^{(-z\sqrt{d})}erfc\left(\frac{z}{2}\sqrt{\frac{\mathrm{Pr}}{t}} - \sqrt{\frac{dt}{\mathrm{Pr}}}\right)\right)$$

$$\phi(z,t) = \frac{1}{2}\left(\left(t + \frac{z}{2}\sqrt{\frac{\mathrm{Sc}}{\mathrm{Kc}}}\right)e^{\left(z\sqrt{\frac{\mathrm{Sc}}{\mathrm{Kc}}}\right)}erfc\left(\frac{z}{2}\sqrt{\frac{\mathrm{Sc}}{t}} + \sqrt{\mathrm{Kc}t}\right) + \left(t - \frac{z}{2}\sqrt{\frac{\mathrm{Sc}}{\mathrm{Kc}}}\right)e^{\left(-z\sqrt{\frac{\mathrm{Sc}}{\mathrm{Kc}}}\right)}erfc\left(\frac{z}{2}\sqrt{\frac{\mathrm{Sc}}{t}} - \sqrt{\mathrm{Kc}t}\right)\right)$$

$$\tau = e^{(at)}\left(\sqrt{\lambda+a}\left(1 - erfc\sqrt{(\lambda+a)t}\right) + \frac{1}{\sqrt{\pi t}}e^{(-t(\lambda+a))}\right) + \left(\frac{\mathrm{Grcos}\alpha}{(1-\mathrm{Pr})}\right)\left(\frac{e^{(\alpha_1 t)}}{\alpha_1^2}\left\{\sqrt{\lambda+\alpha_1}\left(erfc\sqrt{(\lambda+\alpha_1)t} - 1\right) - \frac{1}{\sqrt{\pi t}}e^{(-t(\lambda+\alpha_1))}\right.\right.$$

$$\left.\left. - \sqrt{d+\mathrm{Pr}\alpha_1}\left(erfc\sqrt{\left(\frac{d}{\mathrm{Pr}} + \alpha_1\right)t} - 1\right) + \sqrt{\frac{\mathrm{Pr}}{\pi t}}e^{\left(-t\left(\frac{d}{\mathrm{Pr}}+\alpha_1\right)\right)}\right\} + \frac{1}{2\alpha_1\sqrt{\lambda}}\left(1 - erfc\sqrt{\lambda t}\right) + \frac{1}{\alpha_1}\left(t + \frac{1}{\alpha_1}\right)\left\{\sqrt{\lambda}\left(1 - erfc\sqrt{\lambda t}\right) + \frac{1}{\sqrt{\pi t}}e^{(-\lambda t)}\right\}\right)$$

$$-\frac{\mathrm{Pr}}{2\alpha_1\sqrt{d}}\left(1-erfc\sqrt{\frac{dt}{\mathrm{Pr}}}\right)-\frac{1}{\alpha_1}\left(t+\frac{1}{\alpha_1}\right)\times\left\{\sqrt{d}\left(1-erfc\sqrt{\frac{dt}{\mathrm{Pr}}}\right)+\sqrt{\frac{\mathrm{Pr}}{\pi t}}e^{\left(-\frac{dt}{\mathrm{Pr}}\right)}\right\}+\left(\frac{\mathrm{Gm}\cos\alpha}{(1-\mathrm{Sc})}\right)$$

$$\left(\frac{e^{(\alpha_2 t)}}{\alpha_2^2}\left\{\sqrt{\lambda+\alpha_2}\left(erfc\sqrt{(\lambda+\alpha_2)t}-1\right)-\frac{1}{\sqrt{\pi t}}e^{(-t(\lambda+\alpha_2))}-\sqrt{\mathrm{Sc}(\mathrm{Kc}+\alpha_2)}\left(erfc\sqrt{(\mathrm{Kc}+\alpha_2)t}-1\right)\right.\right.$$

$$\left.\left.+\sqrt{\frac{\mathrm{Sc}}{\pi t}}e^{(-t(\mathrm{Kc}+\alpha_2))}\right\}+\frac{1}{2\alpha_2\sqrt{\lambda}}\left(1-erfc\sqrt{\lambda t}\right)+\frac{1}{\alpha_2}\left(t+\frac{1}{\alpha_2}\right)\left\{\sqrt{\lambda}\left(1-erfc\sqrt{\lambda t}\right)+\frac{1}{\sqrt{\pi t}}e^{(-\lambda t)}\right\}\right.$$

$$-\frac{1}{2\alpha_2}\sqrt{\frac{\mathrm{Sc}}{\mathrm{Kc}}}\left(1-erfc\sqrt{\mathrm{Kc}t}\right)-\frac{1}{\alpha_2}\left(t+\frac{1}{\alpha_2}\right)\times\left\{\sqrt{\mathrm{ScKc}}\left(1-erfc\sqrt{\mathrm{Kc}t}\right)+\sqrt{\frac{\mathrm{Sc}}{\pi t}}e^{(-\mathrm{Kc}t)}\right\}\right)$$

$$Nu=\left(\frac{\mathrm{Pr}}{2\sqrt{d}}+t\sqrt{d}\right)\left(1-erfc\left(\sqrt{\frac{dt}{\mathrm{Pr}}}\right)\right)+\sqrt{\frac{t\mathrm{Pr}}{\pi}}e^{\left(-\frac{dt}{\mathrm{Pr}}\right)}$$

$$Sh=\left(\frac{1}{2}\sqrt{\frac{\mathrm{Sc}}{\mathrm{Kc}}}+t\sqrt{\mathrm{ScKc}}\right)\left(1-erfc\sqrt{\mathrm{Kc}t}\right)+\sqrt{\frac{t\mathrm{Sc}}{\pi}}e^{(-\mathrm{Kc}t)}$$

References

[1] R. Ganapathy, A note on oscillatory Couette flow in a rotating system, ASME J. Appl. Mechs. 61 (1994) 208–209.

[2] J. Maxwell, A treatise on electricity and magnetism, second ed., Oxford University Press, Cambridge, UK, 1904.

[3] H.C. Brinkman, Viscosity of concentrated suspensions and solution, J. Chem. Phys. 20 (1952) 571–581.

[4] H.F. Oztop, E. Abu-Nada, Numerical study of natural convection in partially heated rectangular enclosures with nanofluids, Int. J. Heat Fluid Flow 29 (2008) 1326–1336.

[5] M.A.A. Hamad, I. Pop, Unsteady MHD free convection flow past a vertical permeable flat plate in a rotating frame of reference with constant heat source in a nanofluid, Heat Mass Transf. 7 (2011) 1517–1524.

[6] P.C. Ram, The effects of Hall and ion slip currents on free convective heat generating flow in a rotating fluid, Int. J. Energy Res. 19 (5) (1995) 371–376, https://doi.org/10.1002/er.4440190502.

[7] M.A. Seddeek, The Effects of Hall and ion-Slip Currents on magneto-micropolar fluid and heat transfer over a non-isothermal stretching sheet with suction and blowing, Proc. Royal Soc.: Lond. A 457 (2001) 3039–3050, https://doi.org/10.1098/rspa.2001.0847.

[8] M.A. Seddeek, M.S. Abdelmeguid, Hall and ion slip effects on magneto-micropolar fluid with combined forced and free convection in boundary layer flow over a horizontal plate, J. Korea Soc. Indus. Appl. Math. 8 (2) (2004) 51–73.

[9] B.K. Jha, C.A. Apere, Combined effect of Hall and ion slip currents on unsteady MHD Couette flows in a rotating system, J. Phys. Soc. Jpn. 79 (10) (2010), https://doi.org/10.1143/JPSJ.79.104401 104401.

[10] Z. Uddin, M. Kumar, Hall and ion slip effect on MHD boundary layer flow of a micro polar fluid past a wedge, Scientia Iranica B 20 (3) (2013) 467–476, https://doi.org/10.1016/j.scient.2013.02.013.

[11] R. Ellahi, M.M. Bhatti, I. Pop, Effects of Hall and ion slip on MHD peristaltic flow of Jeffrey fluid in a non-uniform rectangular duct, Int. J. Numer. Methods Heat Fluid Flow 26 (6) (2016) 1802–1820, https://doi.org/10.1108/HFF-02-2015-0045.

[12] M.M. Bhatti, M.A. Abbas, M.M. Rashidi, Effect of Hall and ion slip on peristaltic blood flow of Eyring Powell fluid in a non-uniform porous channel, World J. Modell. Simul. 12 (4) (2016) 268–279.

[13] D. Srinivasacharya, Md. Shafeeurrahman, Hall and ion slip effects on mixed convection flow of nanofluid between two concentric cylinders, J. Assoc. Arab Univ. Basic Appl. Sci. 24 (1) (2017) 223–231, https://doi.org/10.1016/j.jaubas.2017.03.002.

[14] K.S. Jitendra, C.T. Srinivasa, Unsteady natural convection flow of a rotating fluid past an exponential accelerated vertical plate with Hall current, ion-slip and magnetic effect, Multidisc. Model. Mater. Struct. 14 (2) (2018) 216–235, https://doi.org/10.1108/MMMS-06-2017-0045.

[15] G. Sutton, A. Sherman, Engineering Magnetohydrodynamics, Mc Graw Hill, New York, 1965.

[16] M. Veera Krishna, G.S. Reddy, A.J. Chamkha, Hall effects on unsteady MHD oscillatory free convective flow of second grade fluid through porous medium between two vertical plates, Phys. Fluids 30 (2018) 023106, https://doi.org/10.1063/1.5010863.

[17] M. Veera Krishna, A.J. Chamkha, Hall effects on unsteady MHD flow of second grade fluid through porous medium with ramped wall temperature and ramped surface concentration, Phys. Fluids 30 (2018), https://doi.org/10.1063/1.5025542.

[18] M. Veera Krishna, B.V. Swarnalathamma, A.J. Chamkha, Heat and mass transfer on magnetohydrodynamic chemically reacting flow of micropolar fluid through a porous medium with Hall effects, Spec. Top. Rev. Porous Media – Int. J. 9 (4) (2018) 347–364, https://doi.org/10.1615/SpecialTopicsRevPorousMedia.2018024579.

[19] M. Veera Krishna, A.J. Chamkha, Hall effects on MHD Squeezing flow of a water based nano fluid between two parallel disks, J. Porous Media 22 (2) (2019) 209–223, https://doi.org/10.1615/JPorMedia. 2018028721.

[20] M. Veera Krishna, K. Bharathi, A.J. Chamkha, Hall effects on MHD peristaltic flow of Jeffrey fluid through porous medium in a vertical stratum, Int. Phenomena Heat Transf. 6 (3) (2019) 253–268, https://doi.org/10.1615/InterfacPhenomHeatTransfer.2019030215.

[21] I.A. Sara, M.M. Bhatti, The study of non-Newtonian nanofluid with hall and ion slip effects on peristaltically induced motion in a non-uniform channel, RSC Adv. 8 (2018) 7904–7915, https://doi.org/10.1039/c7ra13188g.

[22] J.R. Pattnaik, G.C. Dash, S. Singh, Radiation and mass transfer effects on MHD flow through porous medium past an exponentially accelerated inclined plate with variable temperature, Ain Shams Engg. J. 8 (2017) 67–75, https://doi.org/10.1016/j.asej.2015.08.014.

[23] J.L. Bansal, Magneto fluid dynamics of viscous fluids, Jaipur Pub House, Jaipur (India), 1994.

[24] H. Schlichting, K. Gersten, Boundary layer theory, McGraw-Hill Book Co, New York (USA), 1999.

[25] M. Veera Krishna, Ali J. Chamkha, Hall and ion slip effects on MHD rotating boundary layer flow of nanofluid past an infinite vertical plate embedded in a porous medium, Results Phys. 15 (2019) 102652, https://doi.org/10.1016/j.rinp.2019.102652.

[26] M. Veera Krishna, B.V. Swarnalathamma, A.J. Chamkha, Investigations of Soret, Joule and Hall effects on MHD rotating mixed convective flow past an infinite vertical porous plate, J. Ocean Engg. Sci. 4 (3) (2019) 263–275, https://doi.org/10.1016/j.joes.2019.05.002.

[27] H. Ahmad, S.A.M. Mehryan, M. Ghalambaz, Time periodic natural convection heat transfer in a nano-encapsulated phase-change suspension, Int. J. Mech. Sci. 166 (2019), https://doi.org/10.1016/j.ijmecsci.2019.105243 105243.
[28] M. Ghalambaz, T. Groşan, I. Pop, Mixed convection boundary layer flow and heat transfer over a vertical plate embedded in a porous medium filled with a suspension of nano-encapsulated phase change materials, J. Mol. Liquids 293 (2019), https://doi.org/10.1016/j.molliq.2019.111432 111432.
[29] Z. Hossein, A. Noghrehabadi, M. Ghalambaz, I. Pop, Natural convection boundary layer flow over a horizontal plate embedded in a porous medium saturated with a nanofluid: Case of variable thermophysical properties, Trans. Porous Media 107 (1) (2015) 153–170, https://doi.org/10.1007/s11242-014-0430-4.
[30] Aminreza Noghrehabadi, Ehsan Izadpanahi, M. Ghalambaz, Analyze of fluid flow and heat transfer of nanofluids over a stretching sheet near the extrusion slit, Comp. Fluids 100 (2014) 227–236, https://doi.org/10.1016/j.compfluid.2014.05.013.
[31] M. Ghalambaz, M.H.Z. Seyed, S.A.M. Mehryan, I. Pop, D. Wen, Analysis of melting behavior of PCMs in a cavity subject to a non-uniform magnetic field using a moving grid technique, Appl. Math. Model. 77 (2020) 1996–11953, https://doi.org/10.1016/j.apm.2019.09.015.
[32] M. Ghalambaz, M. Sabour, I. Pop, D. Wen, Free convection heat transfer of MgO-MWCNTs/EG hybrid nanofluid in a porous complex shaped cavity with MHD and thermal radiation effects, Int. J. Numer. Meth. Heat Fluid Flow 29 (11) (2019) 4349–4376, https://doi.org/10.1108/HFF-04-2019-0339.
[33] M. Ghalambaz, D. Ali, Z. Hossein, A.J. Chamkha, MHD phase change heat transfer in an inclined enclosure: Effect of a magnetic field and cavity inclination, Numer. Heat Transf. Appl. 71 (1) (2017) 1–19, https://doi.org/10.1080/10407782.2016.1244397.
[34] M. Ghalambaz, M. Sabour, S. Sazgara, I. Pop, R. Trâmbiţaş, Insight into the dynamics of ferrohydrodynamic (FHD) and magnetohydrodynamic (MHD) nanofluids inside a hexagonal cavity in the presence of a non-uniform magnetic field, J. Magne. Magnetic Mater. 497 (2020), https://doi.org/10.1016/j.jmmm.2019.166024 166024.
[35] A.T. Mohamed, Numerical simulation of double diffusive natural convection in rectangular enclosure in the presences of magnetic field and heat source, Int. J. Thermal Sci. 47 (3) (2008) 237–248, https://doi.org/10.1016/j.ijthermalsci.2007.02.003.
[36] A.T. Mohamed, F.E. Ahmed, Z.M. Enass, Numerical simulation of double-diffusive natural convective flow in an inclined rectangular enclosure in the presence of magnetic field and heat source, Int. J. Therm. Sci. 52 (1) (2012) 161–175, https://doi.org/10.1016/j.ijthermalsci.2011.09.006.
[37] A.T. Mohamed, W.M. El-Maghlany, Augmentation of natural convective heat transfer in square cavity by utilizing nanofluids in the presence of magnetic field and uniform heat generation/absorption, Int. J. Therm. Sci. 58 (2012) 130–142, https://doi.org/10.1016/j.ijthermalsci.2012.02.029.
[38] A.T. Mohamed, A.F. Elsafty, M.Z. Elfeky, E.Z. El-Gazzar, Numerical simulation of double-diffusive natural convective flow in an inclined rectangular enclosure in the presence of magnetic field and heat source, part A: Effect of Rayleigh number and inclination angle, Alex. Engg. J. 50 (4) (2011) 269–282, https://doi.org/10.1016/j.aej.2010.05.001.
[39] Khilap Singhm, Alok Kumar Pandey, Manoj Kumar, Analytical approach to stagnation-point flow and heat transfer of a micropolar fluid via a permeable shrinking sheet with slip and convective boundary conditions, Heat Transf. Res. 50 (8) (2019) 739–756, https://doi.org/10.1615/HeatTransRes. 2018024647.
[40] Padam Singh, Alok Kumar Pandey, Manoj Kumar, Forced convection in MHD slip flow of alumina water nanofluid over a flat plate, J. Enhanced Heat Transf. 23 (6) (2016) 487–497, https://doi.org/10.1615/JEnhHeatTransf. 2018025485.
[41] Alok Kumar Pandey, Manoj Kumar, Effect of viscous dissipation and suction/injection on MHD nanofluid flow over a wedge with porous medium and slip, Alex. Engg. J. 55 (4) (2016) 3115–3123, https://doi.org/10.1016/j.aej.2016.08.018.
[42] Himanshu Upreti, Alok Kumar Pandey, Manoj Kumar, MHD flow of Ag-water nanofluid over a flat porous plate with viscous-Ohmic dissipation, suction/injection and heat generation/absorption, Alex. Engg. J. 57 (3) (2018) 1839–1847, https://doi.org/10.1016/j.aej.2017.03.018.
[43] Alok Kumar Pandey, Manoj Kumar, MHD flow inside a stretching/shrinking convergent/divergent channel with heat generation/absorption and viscous-Ohmic dissipation utilizing Cu−water nanofluid, Comput. Therm. Sci.: An Int. J. 10 (5) (2018) 457–471, https://doi.org/10.1615/ComputThermalScien. 2018020807.
[44] Alok Kumar Pandey, Manoj Kumar, Natural convection and thermal radiation influence on nanofluid flow over a stretching cylinder in a porous medium with viscous dissipation, Alexandria Eng. J. 56 (1) (2017) 55–62, https://doi.org/10.1016/j.aej.2016.08.035.
[45] Ashish Mishra, Alok Kumar Pandey, Manoj Kumar, Velocity, thermal and concentration slip effects on MHD silver-water nanofluid past a permeable cone with suction/injection and viscous-Ohmic dissipation, Heat Transf. Res. 50 (14) (2019) 1351–1367, https://doi.org/10.1615/HeatTransRes. 2018020420.
[46] Alok Kumar Pandey, Manoj Kumar, Boundary layer flow and heat transfer analysis on Cu-water nanofluid flow over a stretching cylinder with slip, Alex. Engg. J. 56 (4) (2017) 671–677, https://doi.org/10.1016/j.aej.2017.01.017.